Published in final edited form as:
Eur J Mass Spectrom (Chichester). 2019 February 01; 25(1): 122–132. doi:10.1177/1469066718803307.

Infrared Multiple Photon Dissociation of Cesium Iodide Clusters Doped with Mono-, Di- and Triglycine

Jakob Heller, **Milan Ončák**, **Nina K. Bersenkowitsch**, **Christian van der Linde**, **Martin K. Beyer**
Institut für Ionenphysik und Angewandte Physik, Leopold-Franzens-Universität Innsbruck, Technikerstraße 25, 6020 Innsbruck, Austria

Abstract

Charged cesium iodide clusters doped with mono-, di- and triglycine serve as a model system for sea salt aerosols containing biological molecules. Here, we investigate reactions of these complexes under infrared irradiation, with spectra obtained by infrared multiple photon dissociation (IRMPD). The cluster ions are generated via electrospray ionization and analyzed in the cell of a Fourier Transform Ion Cyclotron Resonance (FT-ICR) Mass Spectrometer. Depending on the cluster size and peptide length, loss of HI or loss of a glycine unit is observed. The experimental measurements are supported by quantum chemical calculations. We show that N-H and O-H stretching modes dominate the spectrum, with large shifts depending on local interactions, namely due to interaction with iodide anions or intramolecular hydrogen bonding. Both experiment and theory indicate that several isomers are present in the experimental mixture, with different IR fingerprints as well as dissociation pathways.

Introduction

The interaction of ions with biomolecules plays an important role in many biological processes. Infrared multiple photon (IRMPD) spectroscopy along with quantum chemical computations allows probing the conformation of these complexes in the gas phase. Dunbar *et al.* studied a series of complexes of small peptides with alkali, alkaline earth and transition metal ions.[1–21] Other groups studied complexes of peptides with alkali metals like sodium and potassium,[22,23] with halides,[24] and even with lanthanide ions.[25]

These studies were limited to the interaction of amino acids and peptides with individual metal ions while we did not find any studies addressing the interaction of amino acids or peptides with salt clusters. In particular alkali halide clusters are ideal gas phase models for sea salt aerosols, which are an essential component of atmospheric chemistry in marine

martin.beyer@uibk.ac.at.

Europe PMC Funders Author Manuscripts

regions.[26] Consisting mainly of sodium chloride, water and organic matter from the sea surface microlayer, sea salt aerosols are released to the atmosphere from the ocean surface by the bursting of air bubbles generated by the ocean wind.[27] Field studies showed a high concentration of sodium compared to chloride in atmospheric aerosol samples.[28,29] This chloride deficit can be explained by the reaction of sea salt with trace gases like HONO and HNO_3, where chloride is released as gaseous HCl.[30,28,31–33] We have recently studied the influence of the salt environment on the photodissociation of glyoxylate[34] and pyruvate.[35] Very little is known on the effect of a salt environment on the infrared spectra of organic compounds, and our recent work addressed this issue for camphor, formate and pyruvate embedded in sodium iodide clusters.[35] We were able to show that IRMPD in combination with quantum chemistry can help to identify the binding motifs of the organic molecules to the salt cluster.

Alkali halide clusters in the gas phase were extensively studied by Whetten, Martin and Lintuluoto.[36–39] Especially the adsorption of ammonia[40,41] and water[42–46] to various alkali halides was investigated by several groups. The collision cross section of sodium iodide clusters was studied by Ouyang et al. using mobility measurements,[47] while Blades et al. investigated the hydration energy of Na_2I^+.[48] The structures and stabilities of neutral and singly charged sodium iodide clusters were investigated with *ab initio* methods by Aguado et al.[49,50] Misaizu et al. examined sodium iodide clusters with adsorbed methanol using photodissociation experiments and DFT methods.[51] UV spectra of cesium iodide $Cs_{n+1}I_n^+$ were examined by Li and Whetten for $n = 1–13$.[52]

In the present work, complexes of positively charged cesium iodide clusters with amino acids and peptides serve as a model system to investigate the reactions of sea salt aerosols with biological molecules under the influence of infrared radiation. CsI was chosen instead of NaCl because the target cluster ions containing intact peptide molecules were obtained with higher signal intensities. A powerful tool to investigate infrared driven reactions[53–56] is infrared multiple photon dissociation (IRMPD).[57] In IRMPD, a vibrational mode of the ion is pumped with resonant light and the complex is successively heated by intramolecular vibrational redistribution (IVR). The ion dissociates as soon as it has reached sufficient internal energy. Mass and intensity of the fragments are recorded by a mass spectrometer. The fragment intensities as a function of wavelength yield the infrared spectrum of the complex, providing structural information. We also show that biomolecules containing carboxyl groups can contribute to the release of hydrogen halides from salt clusters.

Experimental and theoretical methods

The experiments are performed on a commercial Bruker APEX Qe 9.4T Fourier Transform-Ion Cyclotron Mass Spectrometer (FT-ICR MS). Ions are produced by electrospray ionization (ESI) and transferred via ion funnels, quadrupole, hexapole collision cell and ion optics into the ICR cell where they are stored for irradiation. Complexes of interest are coarsely mass selected in the quadrupole mass filter, followed by resonant ejection of unwanted ions from the ICR cell.

Chemicals are purchased from Sigma Aldrich and are dissolved in 1:1 H_2O/CH_3OH at a concentration of 3 mmol CsI/3 mmol G (Glycine, $C_2H_5NO_2$), 2.5 mmol CsI/1 mmol GG (Diglycine, $C_4H_8N_2O_3$), and 2.5 mmol CsI/1 mmol GGG (Triglyine, $C_6H_{11}N_3O_4$), respectively. IRMPD spectra of these complexes are measured in a range from 2700 nm to 3800 nm (corresponding to 3704 cm^{-1} to 2632 cm^{-1}), with 3 nm step width and typically 1 s irradiation time.

Mass selected ions are irradiated by light provided by an EKSPLA NT277 Optical Parametric Oscillator (OPO), tunable from 2500 from 4475 nm, which is coupled to the ICR cell via a CaF_2 window as described before.[34,58,59] The pulsed laser systems operates with 1000 Hz repetition rate, which on the time scale of the ICR instrument is quasi-continuous wave (cw), with a wavelength dependent quasi-cw power of 85-125 mW in the wavelength range of interest. To rule out an impact of power fluctuations on the results, the power spectrum of the laser was measured before each IRMPD spectrum. A mechanical shutter controls the irradiation time.

To extract quantitative IR absorption cross sections from the photofragment intensities, we assume that the absorption cross section σ does not change after photon absorption, and assume that radiative cooling is negligible. We can then describe IRMPD as a series of first-order reactions with the rate coefficient $\sigma\Phi$, where we divide the ion population into fractions I_j that have absorbed j photons. Assuming that dissociation occurs upon absorption of the k^{th} photon, we look at a set of differential equations (1)–(3).

$$dI_0 = -I_0\sigma\Phi dt \tag{1}$$

$$dI_j = I_{j-1}\sigma\Phi dt - I_j\sigma\Phi dt \quad \text{for } 0 < j < k \tag{2}$$

$$dI_k = I_{k-1}\sigma\Phi dt \tag{3}$$

Here, I_k is the sum of all fragment intensities, and Φ is the cw photon flux. For practical data evaluation, we generate a lookup table with intensities I_k as a function of $\sigma\Phi t$. This allows us to extract σ_k with the parameters Φ and t known from experiment, where σ_k denotes the cross section if dissociation occurs after absorption of k photons. See SI, Figure S1, for a graphical representation of the lookup table.

This approach is indeed very simplified, and a more sophisticated treatment would yield more reliable results, like e.g. the accurate modeling of IRMPD spectra including anharmonicities by Parneix,[60,61] approach outlined in the classical works by Y.T. Lee and co-workers,[62] the statistical description of inhomogeneous line broadening by Letokhov and co-workers[63] or the effects of anharmonicities discussed by Oomens, Sartakov, Meijer and von Helden.[64] However, the situation in our work where relatively weakly bound non-covalent complexes with dissociation barriers around 100 kJ/mol are studied, is quite different from the IRMPD work of strongly bound organic ions, e.g. the photodissociation of cationic polyaromatic hydrocarbons.[65] Given the boundary conditions, this simple model

yields cross sections that are in the range of the actual value, and we believe that meaningful additional information is obtained compared to reporting pure IRMPD yields.

To test for the presence of isomers and to verify that the laser beam overlaps with the ion cloud,[66,67] dissociation kinetics at selected wavelengths is recorded with and without irradiation of the complexes with irradiation times up to 10 s. The kinetics data are fitted assuming a pseudo-first order rate law.

Quantum chemical calculations were performed in order to retrieve energetics and analyze the relationship between structure and IR spectra. The investigated clusters have very floppy structures, and both their relative energies and IR transitions can be expected to be sensitive to small changes in structure. At the same time, the position of IR peaks will depend on subtle changes in charge distribution. Therefore, we did benchmarking on $(Cs_3I_2)^+G$ isomers (see Table S1 and Figure S2), using the MP2 method and three different DFT functionals, namely B3LYP, M06 and M06L,[68] along with the def2TZVP basis set. In order to search for a more efficient basis set for the MP2 method and as Cs^+ and I^- ions are expected to keep their ionic character also in complexes, we used ECP54SDF[69] and ECP46MDF[70] basis sets for Cs and I, respectively, along with def2SVP basis set on all other atoms, further denoted as “def2SVP+ECP(Cs,I)”. From Table S1 and Figure S2, it can be seen that the relative energies of $(Cs_3I_2)^+G$ isomers are well reproduced with both M06 and M06L functionals; however, the differences in the position of the IR peaks for all DFT functionals with respect to the MP2 method are considerable, mainly in the position of the O-H vibration. The usage of the small basis set along with the MP2 method can be expected to fail when describing the relative energies of different CsI cluster structures, compare e.g. relative energies of isomers **I**, **IV** and **VI** vs. **III** and **V** in Table S1. However, as we are interested here predominantly in IR spectra, we decided to use the MP2/def2SVP+ECP(Cs,I) method since it yields spectra that are most consistent with the MP2/def2TZVP results. At the same time, the reaction energies calculated at the MP2/def2SVP+ECP(Cs,I) level are close to the ones retrieved at the M06/def2TZVP level (see Table 1); besides basis set effects, the differences can be attributed to the dispersion interaction that is not accounted for at the M06 level. Finally, due to the vast conformation space, the localized isomers represent only possible bonding patterns and the inclusion of entropy might also further change their relative stability; information on their energy ordering should be taken with caution even when using advanced methods. All reported energies include zero-point corrections, using the calculated harmonic frequencies without scaling factor.

For broadening of IR peaks, Lorentzian functions with a full width at half maximum (FWHM) of 20 cm^{-1} were employed. The scaling factor for IR spectra was chosen individually for each method to reproduce the position of a free O-H group in the glycine molecule (~ 3600 cm^{-1}). The Gaussian program package[71] was used for all calculations.

Results and Discussion

In the mass spectra of CsI-GG and CsI-GGG solutions, see Figure S3, neutral peptide molecules attached to cesium iodide clusters are observed, $(Cs_{n+1}I_n)^+GG$ with $n = 0–2$ and $(Cs_{n+1}I_n)^+GGG$ with n = 0–3, as well as clusters containing two peptide molecules. Also,

clusters of $(Cs_{m+2}I_m)^{2+}(GG\text{-}H)^-$, $m = 0–2$, and $(Cs_{m+2}I_m)^{2+}(GGG\text{-}H)^-$, $m = 0–3$, composition are found, where the deprotonated peptide replaces iodide. An additional neutral peptide molecule may be bound to these complexes. For the neutral amino acid G, only $(Cs_3I_2)^+G$ is observed in the investigated mass range, while deprotonated G occurs as $(Cs_{m+2}I_m)^{2+}(G\text{-}H)^-$, $m = 0–3$.

We have chosen $(Cs_3I_2)^+G$, $(Cs_3I_2)^+GG$, $(Cs_3I_2)^+GGG$, $(Cs_2I)^+GG$ and $(Cs_2I)^+GGG$ for IRMPD experiments on mass selected clusters. Calculated structures of low-lying isomers are shown in Figure 1. Upon irradiation with IR light, two fragmentation channels are observed, the loss of HI and the loss of the peptide or amino acid, e.g. for $(Cs_3I_2)^+GG$:

$$(Cs_3I_2)^+GG \rightarrow (Cs_3I_2)^+(GG\text{-}H)^- + HI \quad (4)$$

$$(Cs_3I_2)^+GG \rightarrow (Cs_3I_2)^+ + GG \quad (5)$$

The respective dissociation energies as calculated at two different levels of theory are collected in Table 1. For HI elimination (4), an additional barrier may be expected due to possible transition states along the reaction path and the reorganization energy of the cluster to bring it into a suitable geometry for proton transfer. We therefore investigated the reaction path of HI elimination for all ions studied, starting from isomers with a pronounced OH…I interaction (see relaxed dissociation scans at the B3LYP/def2TZVP level of theory in Figure S12). In all cases, no stationary points were found along the reaction path, and no evidence for any barrier above the dissociation asymptotes was found.

For simple dissociation (5), the activation barrier is expected to be equal to the overall reaction energy, with only limited reorganization energy. All energies are in the range of 100 kJ/mol, i.e. at a photon energy of 3000 cm^{-1} (~36 kJ/mol) about 3–4 photons are needed for the reactions to occur when thermal energy is ignored. However, the ions are thermalized in the hexapole collision cell and by exchange of black-body infrared radiation in the ICR cell, which reduces the required extra energy to 2–3 photons. Since the dissociation kinetics were all fitted well with sequential absorption of two photons, all experimental spectra were analyzed with the assumption that two photons are needed for dissociation. Spectra analyzed with up to five absorbed photons are available in the Supporting Information (Figures S7–S11). The major difference is a shift of the absolute absorption cross section to higher values with increasing number of photons.

We will start our discussion of IR spectra with the simplest system, $(Cs_3I_2)^+G$. In this case, only evaporation of G was observed, calculated as being by ~10 kJ/mol less endothermic than HI evaporation at the MP2 level of theory (see Table 1). The measured IRMPD spectrum of $(Cs_3I_2)^+G$ is shown in Figure 2a. The spectrum shows one broad band at ~2700–3200 cm^{-1} and two sharper bands at 3380 cm^{-1} and 3440 cm^{-1}. Based on the comparison with calculated IR spectra in Figure 2b, the broad band is assigned to the O-H stretching mode of the intramolecular O-H…NH_2 hydrogen bond in glycine. This structural motif is present in isomers **I**, **III**, and **V**. The width of the band is typical for strongly

activated O-H bonds, in this case by the interaction with NH_2, together with the room temperature thermal energy of the system. When this interaction is absent (isomers **IV**, **VI**), the free O-H vibration at ~3600 cm^{-1} is present in the calculated spectrum; it is, however, not observed in the experiment. Alternatively, the O-H moiety might interact with I^- (isomer **II**), leading to higher intensities and a blue-shift with respect to the experimental spectrum. The position of the sharp peaks at 3380 cm^{-1} and 3440 cm^{-1} matches well with N-H vibrations in the calculations. The weak C-H vibrational fingerprint at ~2900 cm^{-1} is hidden below the intense O-H absorption. The glycine molecule seems to interact with the cluster mainly via the carboxyl group.

Figure 2c shows the measured IRMPD spectrum of $(Cs_3I_2)^+GG$. The observed channel here is HI evaporation, in agreement with thermochemical calculations (Table 1). Again, a broad band at ~2900–3300 cm^{-1} is observed, indicating strongly interacting OH group. Furthermore, we see an intense sharp band at 3394 cm^{-1}, two small bands at 3440 and 3487 cm^{-1} and the unperturbed O-H vibration at 3577 cm^{-1}. The calculated spectra in Figure 2d offer a less clear interpretation than in the previous case. The broad band at ~2900–3300 cm^{-1} can be interpreted to arise due to OH interacting either with an I^- ion (isomers **III**, **V**) or due to intramolecular OH…NH_2 hydrogen bonding of the diglycine (isomer **VI**). The signal is also consistent with formation of a zwitterionic structure (isomer **VII**) where NH3+ interacts with I^-. A combination of these binding patterns can build up the diffuse band. The sharp band at ~3400 cm^{-1} fits to the O-H stretching mode shifted by the interaction with I^- (isomer **I**). Another possibility is the interaction of a backbone N-H group with I^- (isomer **II**). The three less intense peaks at 3394, 3440 and 3577 cm^{-1} are assigned to unperturbed N-H and O-H vibrations, similarly to $(Cs_3I_2)^+G$ discussed above.

Measured and calculated IRMPD spectra of $(Cs_3I_2)^+GGG$ are shown in Figure 2e,f. HI evaporation is again observed, being calculated to be about 50–80 kJ/mol less endothermic than GGG loss. The IR spectrum is similar to the one of $(Cs_3I_2)^+GG$ (Figure 2c), the broad band at 2800–3300 cm^{-1} is however slightly more diffuse and the sharp peak at 2940 cm^{-1} is better resolved. Our interpretation is thus similar: We expect the broad band to be composed predominantly of O-H interaction, here with I^- ions (isomers **I**, **II**, **IV**), the sharp bands arise then due to N-H vibrations, and a free O-H band is located at 3577 cm^{-1} (isomers **III**, **V**). The particularly sharp band at 2940 cm^{-1} can be assigned to one specific O-H interaction that gains intensity through interaction with the salt cluster (e.g. in isomer **IV**).

With respect to absolute intensities, it can be seen that our calculations reproduce the trend observed in the experiment, with a low intensity for $(Cs_3I_2)^+G$ (except for isomer II) and about equal intensity for $(Cs_3I_2)^+GG$ and $(Cs_3I_2)^+GGG$. As the calculated vibrational spectrum is empirically broadened, it cannot reproduce the broad bands seen in the experiment. If we used higher FWHM, the calculated intensity would decrease and semi-quantitative agreement with IRMPD spectra would be reached, always assuming that two photons are needed for dissociation.

Data for $(Cs_2I)^+GG$ are presented in Figure 3a,b. GG evaporation is the only channel observed in the spectra measured with 1 s irradiation time. HI evaporation is a minor product channel and only visible at longer irradiation times, see below in the kinetics. While the

calculations predict that both channels have about the same energy; most likely HI evaporation channel is slowed down by the reorganisation energy or due to entropic effects in addition to the reaction endothermicity. The broad peak with its maximum at ~2950 cm^{-1} is again assigned to the O-H stretching mode shifted by intramolecular OH…NH_2 hydrogen bonding in the diglycine molecule (isomer **IV**) as well as OH…I^- interaction (isomers **I**, **VI**). The intense absorption at 3387 cm^{-1} is assigned to the O-H stretching mode of the OH…I^- hydrogen bond in isomer **II**. At 3577 cm^{-1}, a well-resolved unperturbed O-H vibration can be seen, as present in isomers **III** and **V**.

Figure 3c,d shows the measured and calculated IRMPD spectra for $(Cs_2I)^+$GGG. Here the main fragment that contributes to the total IRMPD yield is the loss of HI, resulting in Cs_2^{2+} $(GGG-H)^-$, in agreement with the calculated energetics, Table 1. GGG loss is only observed at longer irradiation times. The spectrum is very similar to the one of $(Cs_2I)^+$GG and we interpret the observed bands in a similar fashion. The O-H peak of the most stable isomer calculated with triglycine forming a cycle (**I**) lies at ~2700 cm^{-1}, while the experimental maximum is observed at ~2900 cm^{-1}. This indicates that we reach the limits of our computational approach as small changes in the OH…NH_2 distance lead to a considerable shift in the peak position. The peak at 3384 cm^{-1} is attributed to the OH…I^- interaction in isomer **III**. Peaks at 3477 and 3577 cm^{-1} represent free N-H and O-H bonds, respectively.

For complexes with $(Cs_2I)^+$, the calculated relative intensities can again reasonably reproduce the experimental measurements, predicting similar intensity for both $(Cs_2I)^+$GG and $(Cs_2I)^+$GGG. Due to extreme peak broadening and the presence of multiple isomers, quantitative agreement cannot be expected.

The length of the peptide seems to have an influence on the dominant fragmentation channel, as seen for $(Cs_3I_2)^+$ complexes. For $(Cs_3I_2)^+$G, the loss of G is dominant, while $(Cs_3I_2)^+$GG and $(Cs_3I_2)^+$GGG preferentially lose HI. Again, in the spectra the minor channel lies below the noise level, but becomes evident at longer irradiation times in the kinetics plots, see SI. We can trace this trend to a stronger interaction between the salt cluster and the peptide backbone. As longer peptides contain more amide bonds forming a strongly bound complex, preferential loss of HI is observed with the growing chain, see also Table 1. Complexes of $(Cs_2I)^+$ show a similar behavior. The dominant channel for $(Cs_2I)^+$GG is the loss of GG, while for $(Cs_2I)^+$GGG, HI elimination is dominant.

In Figure 4, all measured IRMPD spectra are compared, the top row shows $(Cs_2I)^+$ and the bottom row $(Cs_3I_2)^+$ complexes. For all ions except for $(Cs_3I_2)^+$G, the free O-H vibration is located at 3576 cm^{-1}. The free O-H absorption is more pronounced for $(Cs_2I)^+$ than $(Cs_3I_2)^+$ complexes. The additional CsI unit in $(Cs_3I_2)^+$ increases the probability for H-I interaction and therefore diminishes the contribution of isomers with free OH absorption to the total ion population.

Only limited absorption at about 3480 cm^{-1} is observed for $(Cs_3I_2)^+$G, and it is considerably stronger for GGG than for GG complexes. This supports the assignment of this peak to unperturbed N-H vibrations of the backbone. In the range of 3360–3460 cm^{-1}, however, the vibrations of the terminal NH_2 group and the perturbed OH vibration are localized.

According to the calculations, only the distinct OH…I^- interaction found in several isomers can explain the high intensity of the prominent feature at 3380 cm^{-1}, which is present at the same position for all peptide complexes. Between 2915 cm^{-1} and 2970 cm^{-1}, two peaks are seen for CsI peptide complexes and are on the same position for every complex. They most likely originate from specific OH interactions.

All spectra are dominated by a very broad absorption from around 2700 to 3500 cm^{-1}. For $(Cs_3I_2)^+$ complexes, the center of this absorption is at higher wavenumbers and is more intense than for $(Cs_2I)^+$. As the intensity of the unperturbed OH vibration is smaller for $(Cs_3I_2)^+$ complexes, it is assumed that I-H interaction is stronger here than for $(Cs_2I)^+$ complexes. Therefore, the OH vibrations gain intensity and the position of the absorption is blue shifted because of the smaller I-H distance. For $(Cs_3I_2)^+$G, this absorption is even broader than for peptide complexes and centered at lower wavenumbers. This indicates that the CsI-amino acid interaction is stronger and the mean I-H distance is lower.

Further evidence that there are several isomers present in the experiment is provided by dissociation kinetics of $(Cs_2I)^+$GGG, measured without irradiation and with irradiation at three different wavelengths (Figure 5). The dominant pathway at all wavelengths is the loss of HI, with the calculated dissociation energies of ~100 kJ/mol (see Table 1). For the second dissociation channel (5), a higher dissociation energy of ~120–150 kJ/mol was calculated.

For the fitting, the fragmentation pathways are described by three different fractions of the precursor: A and B that dissociate along channels (4) and (5), respectively, and a constant that represents the fraction that does not fragment, i.e. ions that are not irradiated with light or isomers that do not absorb at the given irradiation wavelength. Due to the multiple photon dissociation, ions have to heat up before dissociation takes place. The overall dissociation process can be described as follows: A/B → heated A/B → fragmentation. This implies that two photons are sufficient to induce fragmentation.

Figure 5a shows the kinetics without laser irradiation. Both $(Cs_2I)^+$ and $Cs_2^{2+}(GGG\text{-}H)^-$ fragments appear, with relatively low intensity, the majority of the ions staying intact. This indicates that a small fraction of two or more high-energy isomers is present, whose dissociation can be activated by room temperature black-body radiation.[53,72–78] The picture changes completely when the ion is irradiated at 2941 cm^{-1} (Figure 5b). Here, only a small fraction of parent ions stays intact (< 2%), the respective ions either do not absorb at this wavelength or do not overlap with the laser beam.[67,66] The irradiated ions are then transformed almost quantitatively into $Cs_2^{2+}(GGG\text{-}H)^-$ fragments, with only a small fraction reacting by loss of GGG. The heating rate of fraction A, which leads to the $Cs_2^{2+}(GGG\text{-}H)^-$ fragment, is lower than for fraction B. The lower heating rate indicates that the absorption cross section is smaller for this isomer. For longer irradiation times (> 5 s), it seems that the intensity of $(Cs_2I)^+$ reaches a constant value, but the intensity of $Cs_2^{2+}(GGG\text{-}H)^-$ is still rising. This indicates that fraction B is completely dissociated. Since fractions A and B must be treated as independent contributions to the ion population to obtain an acceptable fit, this strongly indicates that at least two isomers are present.

When irradiating at 3390 and 3571 cm^{-1} (Figure 5c,d), a similar situation is observed. For 3390 cm^{-1}, fraction C of the parent ion is fitted to zero, i.e. every parent ion can be dissociated. An induction period is observed for the parent ion $(Cs_2I)^+$GGG as the intensity decreases faster after about 0.5 s. Interestingly, at 3571 cm^{-1}, a large fraction of ions (66%) stays intact. In other words, some $(Cs_2I)^+$GGG isomers present in the measurement do not absorb IR photons at this frequency.

The kinetics fits reveal interesting details about IRMPD of these complexes, even though a complete isomer population analysis[66] is not possible on the basis of the available data. First, all kinetics fit nicely to the sequential absorption of two photons, as only one intermediate is required to fit the data. Since the ions are thermalized at room temperature, with kT = 2.5 kJ mol^{-1}, e.g. isomer **I** of $(Cs_2I)^+$GGG with 15 low-frequency modes below 200 cm^{-1} would possess almost 40 kJ/mol internal energy. Together with two photons in the studied wavelength range, the required activation energy in the range of 100 kJ/mol can be reached. Secondly, the different isomers used in the fits do not interconvert prior absorption of the first photon. They exhibit distinct heating rates, which are not correlated with the contribution of the respective isomer to the total ion population. This is nicely reflected in the kinetics at 3571 cm^{-1}, the frequency of the free OH stretching mode, where the majority of clusters does not absorb.

Conclusions

Complexes of cesium iodide with glycine and the small peptides diglycine and triglycine were generated by electrospray ionization. Infrared multiple photon dissociation spectroscopy was performed with a tunable IR-OPO in the range of 2650 cm^{-1} to 3700 cm^{-1}. We found complexes of CsI with neutral and deprotonated peptides or amino acids. The two investigated CsI cluster sizes $(Cs_2I)^+$ and $(Cs_3I_2)^+$ show different affinity towards peptide or amino acid. No complexes of $(Cs_2I)^+$ with glycine were observed. Diglycine and triglycine can be attached to both cluster sizes. The interaction between the peptide backbone O and Cs atom stabilizes the complexes of the di- and tripeptide.

IRMPD spectra show absorptions over the studied wavelength range. The broad structureless background seen for all structures is interpreted to arise due to O-H interaction with the CsI cluster or intramolecular hydrogen bonding. Some bands could also arise due to N-H bond interaction with the salt cluster. Free N-H and O-H modes were also seen in the spectra. On the other hand, we do not expect IR bands due to C-H modes to appear in the spectrum because their intensity is too low to play a role. In isomers with pronounced OH…I interaction, the position of the O-H stretching mode shifts to the blue with increasing CsI cluster size. Along with this shift, a lower intensity of the unperturbed OH vibration is seen, indicating a stronger interaction of the larger cluster with the peptide. This is also reflected in a higher calculated dissociation energy for peptide evaporation.

Kinetic analysis shows that different isomers are present, which do not interconvert on the timescale of the experiment prior to absorption of the first photon. These are partly associated with different fragmentation channels, a loss of the amino acid or peptide or loss of HI. The dominant fragmentation channel changes with peptide length. $(Cs_2I)^+$GG and

$(Cs_3I_2)^+G$ show the loss of GG and G, respectively, while for all other complexes the loss of HI is dominant.

Supplementary Material

Refer to Web version on PubMed Central for supplementary material.

Acknowledgement

This work was supported by the Austrian Science Fund FWF within the DK-ALM: W1259-$N_2$7. M.O. acknowledges the support through the Lise Meitner Programme of the FWF, project No. M2001-NBL. The computational results presented have been achieved using the HPC infrastructure LEO of the University of Innsbruck. The tunable OPO systems are part of the Innsbruck Laser Core Facility, financed by the Austrian Federal Ministry of Science, Research and Economy.

References

1. Dunbar RC, Berden G, Martens JK, et al. Divalent metal-ion complexes with dipeptide ligands having Phe and His side-chain anchors: effects of sequence, metal ion, and anchor. J Phys Chem A. 2015; 119:9901–9909. [PubMed: 26325483]
2. Dunbar RC, Martens J, Berden G, et al. Complexes of Ni(II) and Cu(II) with small peptides: deciding whether to deprotonate. Phys Chem Chem Phys. 2016; 18:26923–26932. [PubMed: 27711408]
3. Dunbar RC, Polfer NC, Berden G, et al. Metal ion binding to peptides: oxygen or nitrogen sites? Int J Mass Spectrom. 2012; 330–332:71–77.
4. Dunbar RC, Martens J, Berden G, et al. Water microsolvation can switch the binding mode of Ni(II) with small peptides. J Phys Chem Lett. 2017; 8:2634–2638. [PubMed: 28537749]
5. Peckelsen K, Martens J, Berden G, et al. Gas-phase complexes of Ni^{2+} and Ca^{2+} with deprotonated histidylhistidine (HisHis): A model case for polyhistidyl-metal binding motifs. J Mol Spectrosc. 2017; 332:38–44.
6. Dunbar RC, Berden G, Oomens J. How does a small peptide choose how to bind a metal ion? IRMPD and computational survey of CS versus iminol binding preferences. Int J Mass Spectrom. 2013; 354–355:356–364.
7. Dunbar RC, Oomens J, Berden G, et al. Metal ion complexes with HisGly: comparison with PhePhe and PheGly. J Phys Chem A. 2013; 117:5335–5343. [PubMed: 23705999]
8. Dunbar RC, Steill JD, Polfer NC, et al. Metal cation binding to gas-phase pentaalanine: divalent ions restructure the complex. J Phys Chem A. 2013; 117:1094–1101. [PubMed: 22928606]
9. Dunbar RC, Steill JD, Polfer NC, et al. Peptide bond tautomerization induced by divalent metal ions: characterization of the iminol configuration. Angew Chem Int Ed Engl. 2012; 51:4591–4593. [PubMed: 22473902]
10. Dunbar RC, Steill JD, Oomens J. Encapsulation of metal cations by the PhePhe ligand: a cation-π ion cage. J Am Chem Soc. 2011; 133:9376–9386. [PubMed: 21553844]
11. Dunbar RC, Steill JD, Oomens J. Chirality-induced conformational preferences in peptide-metal ion binding revealed by IR spectroscopy. J Am Chem Soc. 2011; 133:1212–1215. [PubMed: 21192647]
12. Dunbar RC, Steill JD, Oomens J. Conformations and vibrational spectroscopy of metal-ion/polylalanine complexes. Int J Mass Spectrom. 2010; 297:107–115.
13. Dunbar RC, Steill JD, Oomens J. Cationized phenylalanine conformations characterized by IRMPD and computation for singly and doubly charged ions. Phys Chem Chem Phys. 2010; 12:13383–13393. [PubMed: 20820591]
14. Dunbar RC, Steill JD, Polfer NC, et al. Peptide length, steric effects, and ion solvation govern zwitterion stabilization in barium-chelated di- and tripeptides. J Phys Chem B. 2009; 113:10552–10554. [PubMed: 19606889]

15. Dunbar RC, Hopkinson AC, Oomens J, et al. Conformation switching in gas-phase complexes of histidine with alkaline earth ions. J Phys Chem B. 2009; 113:10403–10408. [PubMed: 19580301]
16. Dunbar RC, Steill JD, Polfer NC, et al. Dimeric complexes of tryptophan with M^{2+} metal ions. J Phys Chem A. 2009; 113:845–851. [PubMed: 19123780]
17. Polfer NC, Oomens J, Dunbar RC. Alkali metal complexes of the dipeptides PheAla and AlaPhe: IRMPD spectroscopy. ChemPhysChem. 2008; 9:579–589. [PubMed: 18293344]
18. Dunbar RC, Polfer NC, Oomens J. Gas-phase zwitterion stabilization by a metal dication. J Am Chem Soc. 2007; 129:14562–14563. [PubMed: 17985905]
19. Forbes MW, Bush MF, Polfer NC, et al. Infrared spectroscopy of arginine cation complexes: direct observation of gas-phase zwitterions. J Phys Chem A. 2007; 111:11759–11770. [PubMed: 17973465]
20. Polfer NC, Oomens J, Moore DT, et al. Infrared spectroscopy of phenylalanine Ag(I) and Zn(II) complexes in the gas phase. J Am Chem Soc. 2006; 128:517–525. [PubMed: 16402839]
21. Polfer NC, Oomens J, Dunbar RC. IRMPD spectroscopy of metal-ion/tryptophan complexes. Phys Chem Chem Phys. 2006; 8:2744–2751. [PubMed: 16763707]
22. Polfer NC, Paizs B, Snoek LC, et al. Infrared fingerprint spectroscopy and theoretical studies of potassium ion tagged amino acids and peptides in the gas phase. J Am Chem Soc. 2005; 127:8571–8579. [PubMed: 15941293]
23. Balaj O-P, Kapota C, Lemaire J, et al. Vibrational signatures of sodiated oligopeptides (GG–Na^+, GGG–Na^+, AA–Na^+ and AAA–Na^+) in the gas phase. Int J Mass Spectrom. 2008; 269:196–209.
24. Chang TM, Berden G, Oomens J, et al. Halide anion binding to Gly_3 Ala_3 and Leu_3. Int J Mass Spectrom. 2015; 377:440–447.
25. Prell JS, Flick TG, Oomens J, et al. Coordination of trivalent metal cations to peptides: Results from IRMPD spectroscopy and theory. J Phys Chem A. 2010; 114:854–860. [PubMed: 19950916]
26. Finlayson-Pitts, BJ, Pitts, JN. Chemistry of the upper and lower atmosphere: Theory, experiments, and applications. San Diego Calif: Academic Press; 2007.
27. O'Dowd CD, Smith MH, Consterdine IE, et al. Marine aerosol, sea-salt, and the marine sulphur cycle: A short review. Atmos Environ. 1997; 31:73–80.
28. Eldering A, Solomon PA, Salmon LG, et al. Hydrochloric acid: A regional perspective on concentrations and formation in the atmosphere of Southern California. Atmos Environ Part A. 1991; 25:2091–2102.
29. Dasgupta PK, Campbell SW, Al-Horr RS, et al. Conversion of sea salt aerosol to $NaNO_3$ and the production of HCl: Analysis of temporal behavior of aerosol chloride/nitrate and gaseous HCl/HNO_3 concentrations with AIM. Atmos Environ. 2007; 41:4242–4257.
30. Laskin A, Moffet RC, Gilles MK, et al. Tropospheric chemistry of internally mixed sea salt and organic particles: Surprising reactivity of NaCl with weak organic acids. J Geophys Res. 2012; 117
31. Finlayson-Pitts BJ. The tropospheric chemistry of sea salt: a molecular-level view of the chemistry of NaCl and NaBr. Chem Rev. 2003; 103:4801–4822. [PubMed: 14664634]
32. Vogt R, Elliott C, Allen HC, et al. Some new laboratory approaches to studying tropospheric heterogeneous reactions. Atmos Environ. 1996; 30:1729–1737.
33. Laux JM, Hemminger JC, Finlayson-Pitts BJ. Xray photoelectron spectroscopic studies of the heterogenous reaction of gaseous nitric acid with sodium chloride Kinetics and contribution to the chemistry of the marine troposphere. Geophys Res Lett. 2012; 21:1623–1626.
34. Bersenkowitsch NK, Ončák M, van der Linde C, et al. Photochemistry of glyoxylate embedded in sodium chloride clusters, a laboratory model for tropospheric sea-salt aerosols. Phys Chem Chem Phys. 2018; 20:8143–8151. [PubMed: 29517776]
35. Bersenkowitsch NK, Ončák M, Heller J, et al. Photodissociation of Sodium Iodide Clusters Doped with Small Hydrocarbons. Chem Eur J.
36. Whetten RL. Alkali halide nanocrystals. Acc Chem Res. 1993; 26:49–56.
37. Martin TP. Alkali halide clusters and microcrystals. Physics Reports. 1983; 95:167–199.
38. Whetten RL, Homer ML, Li X, et al. Reactions of alkali-halide clusters. Ber Bunsenges Phys Chem. 1992; 96:1120–1125.

39. Lintuluoto M. Theoretical study on the structure and energetics of alkali halide clusters. THEOCHEM. 2001; 540:177–192.
40. Homer ML, Livingston FE, Whetten RL. Molecular adsorption-desorption reactions of ammonia on alkali halide clusters and nanocrystals. J Phys Chem. 1995; 99:7604–7612.
41. Lintuluoto M. Theoretical study on the adsorption of NH_3 to alkali halide clusters. J Phys Chem A. 2000; 104:6817–6823.
42. Fatemi DJ, Bloomfield LA. Photoelectron spectroscopy of sodium iodide clusters containing single hydroxyl ions or water molecules. Phys Rev A. 2002; 66:1607.
43. Zhang Q, Carpenter CJ, Kemper PR, et al. On the dissolution processes of Na_2I^+ and Na_3I^{2+} with the association of water molecules: mechanistic and energetic details. J Am Chem Soc. 2003; 125:3341–3352. [PubMed: 12630890]
44. Barnett RN, Landman U. Water adsorption and reactions on small sodium chloride clusters. J Phys Chem. 1996; 100:13950–13958.
45. Yamabe S, Kouno H, Matsumura K. A mechanism of the ion separation of the NaCl microcrystal via the association of water clusters. J Phys Chem B. 2000; 104:10242–10252.
46. Tsuruta M, Furuya A, Ohno K, et al. Adsorption of small molecules with the hydroxyl group on sodium halide cluster ions. J Phys Chem A. 2010; 114:1432–1436. [PubMed: 20020720]
47. Ouyang H, Larriba-Andaluz C, Oberreit DR, et al. The collision cross sections of iodide salt cluster ions in air via differential mobility analysis-mass spectrometry. J Am Soc Mass Spectrom. 2013; 24:1833–1847. [PubMed: 24026975]
48. Blades AT, Peschke M, Verkerk UH, et al. Hydration energies in the gas phase of select $(MX)_mM^+$ ions, where $M^+ = Na^+$, K^+, Rb^+, Cs^+, NH_4^+ and $X^- = F^-$, Cl^-, Br^-, I^-, NO_2^-, NO_3^-. Observed magic numbers of $(MX)_mM^+$ ions and their possible significance. J Am Chem Soc. 2004; 126:11995–12003. [PubMed: 15382934]
49. Aguado A, Ayuela A, López JM, et al. Theoretical study of small $(NaI)_n$ clusters. J Phys Chem B. 1997; 101:5944–5950.
50. Aguado A, Ayuela A, López JM, et al. Ab initio calculations of structures and stabilities of $(NaI)_nNa^+$ and $(CsI)_nCs^+$ cluster ions. Phys Rev B. 1998; 58:9972–9979.
51. Misaizu F, Tsuruta M, Tsunoyama H, et al. Size-dependent structures of $Na_nI_{n-1}^+$ cluster ions with a methanol adsorbate: a combined study by photodissociation spectroscopy and density-functional theory calculation. J Chem Phys. 2005; 123
52. Li X, Whetten RL. Ultraviolet absorption bands of ionic compound clusters: onset of crystalline structures in $[Cs_{n+1}I_n]^+$ n =1–13. J Chem Phys. 1993; 98:6170–6175.
53. Parry IS, Kartouzian A, Hamilton SM, et al. Chemical reactivity on gas-phase metal clusters driven by blackbody infrared radiation. Angew Chem Int Ed Engl. 2015; 54:1357–1360. [PubMed: 25475369]
54. Hermes AC, Hamilton SM, Cooper GA, et al. Infrared driven CO oxidation reactions on isolated platinum cluster oxides, $Pt_nO_m^+$ Faraday Discuss. 2012; 157:213. [PubMed: 23230771]
55. Hermes AC, Hamilton SM, Hopkins WS, et al. Effects of coadsorbed oxygen on the infrared driven decomposition of N_2O on isolated Rh_5^+ clusters. J Phys Chem Lett. 2011; 2:3053–3057.
56. Hamilton SM, Hopkins WS, Harding DJ, et al. Infrared induced reactivity on the surface of isolated size-selected clusters: dissociation of N_2O on rhodium clusters. J Am Chem Soc. 2010; 132:1448–1449. [PubMed: 20078040]
57. Polfer NC. Infrared multiple photon dissociation spectroscopy of trapped ions. Chem Soc Rev. 2011; 40:2211–2221. [PubMed: 21286594]
58. Lengyel J, Ončák M, Herburger A, et al. Infrared spectroscopy of $O^{\cdot}$- and OH- in water clusters: evidence for fast interconversion between $O^{\cdot}$- and $OH^{\cdot}OH$. Phys Chem Chem Phys. 2017; 19:25346–25351. [PubMed: 28891582]
59. Herburger A, van der Linde C, Beyer MK. Photodissociation spectroscopy of protonated leucine enkephalin. Phys Chem Chem Phys. 2017; 19:10786–10795. [PubMed: 28233882]
60. Calvo F, Parneix P. Amplification of anharmonicities in multiphoton vibrational action spectra. ChemPhysChem. 2012; 13:212–220. [PubMed: 22147536]

61. Parneix P, Basire M, Calvo F. Accurate modeling of infrared multiple photon dissociation spectra: the dynamical role of anharmonicities. J Phys Chem A. 2013; 117:3954–3959. [PubMed: 23581979]
62. Grant ER, Schulz PA, Sudbo AS, et al. Is Multiphoton Dissociation of Molecules a Statistical Thermal Process? Phys Rev Lett. 1978; 40:115–118.
63. Makarov AA, Petrova IY, Ryabov EA, et al. Statistical Inhomogeneous Broadening of Infrared and Raman Transitions in Highly Vibrationally Excited XY 6 Molecules. J Phys Chem A. 1998; 102:1438–1449.
64. Oomens J, Sartakov BG, Meijer G, et al. Gas-phase infrared multiple photon dissociation spectroscopy of mass-selected molecular ions. Int J Mass Spectrom. 2006; 254:1–19.
65. Oomens J, van Roij AJA, Meijer G, et al. Gas-Phase Infrared Photodissociation Spectroscopy of Cationic Polyaromatic Hydrocarbons. Astrophys J. 2000; 542:404–410.
66. Prell JS, Chang TM, Biles JA, et al. Isomer population analysis of gaseous ions from infrared multiple photon dissociation kinetics. J Phys Chem A. 2011; 115:2745–2751. [PubMed: 21410158]
67. Prell JS, Correra TC, Chang TM, et al. Entropy drives an attached water molecule from the C- to N-terminus on protonated proline. J Am Chem Soc. 2010; 132:14733–14735. [PubMed: 20886878]
68. Zhao Y, Truhlar DG. The M06 suite of density functionals for main group thermochemistry, thermochemical kinetics, noncovalent interactions, excited states, and transition elements: two new functionals and systematic testing of four M06-class functionals and 12 other functionals. Theor Chem Account. 2008; 120:215–241.
69. von Szentpály L, Fuentealba P, Preuss H, et al. Pseudopotential calculations on Rb^+_2, Cs^+_2, RbH^+, CsH^+ and the mixed alkali dimer ions. Chem Phys Lett. 1982; 93:555–559.
70. Stoll H, Metz B, Dolg M. Relativistic energy-consistent pseudopotentials–recent developments. J Comput Chem. 2002; 23:767–778. [PubMed: 12012353]
71. Frisch, MJ; Trucks, GW; Schlegel, HB; , et al. Gaussian 09, revision D.01 2013.
72. Balaj OP, Berg CB, Reitmeier SJ, et al. A novel design of a temperature-controlled FT-ICR cell for low-temperature black-body infrared radiative dissociation (BIRD) studies of hydrated ions. Int J Mass Spectrom. 2009; 279:5–9.
73. Dunbar RC. BIRD (blackbody infrared radiative dissociation): evolution, principles, and applications. Mass Spectrom Rev. 2004; 23:127–158. [PubMed: 14732935]
74. Fox BS, Beyer MK, Bondybey VE. Black body fragmentation of cationic ammonia clusters. J Phys Chem A. 2001; 105:6386–6392.
75. Schnier PD, Price WD, Jockusch RA, et al. Blackbody infrared radiative dissociation of bradykinin and its analogues: energetics, dynamics, and evidence for salt-bridge structures in the gas phase. J Am Chem Soc. 1996; 118:7178–7189. [PubMed: 16525512]
76. Sena M, Riveros JM. The unimolecular dissociation of the molecular ion of acetophenone induced by thermal-radiation. Rapid Commun Mass Spectrom. 1994; 8:1031–1034.
77. Thölmann D, Tonner DS, McMahon TB. Spontaneous unimolecular dissociation of small cluster ions, $(H_3O^+)L_n$ and $Cl^-(H_2O)_n$ (n=2-4), under Fourier transform ion cyclotron resonance conditions. J Phys Chem. 1994; 98:2002–2004.
78. Schindler T, Berg C, Niedner-Schatteburg G, et al. Protonated water clusters and their black body radiation induced fragmentation. Chem Phys Lett. 1996; 250:301–308.

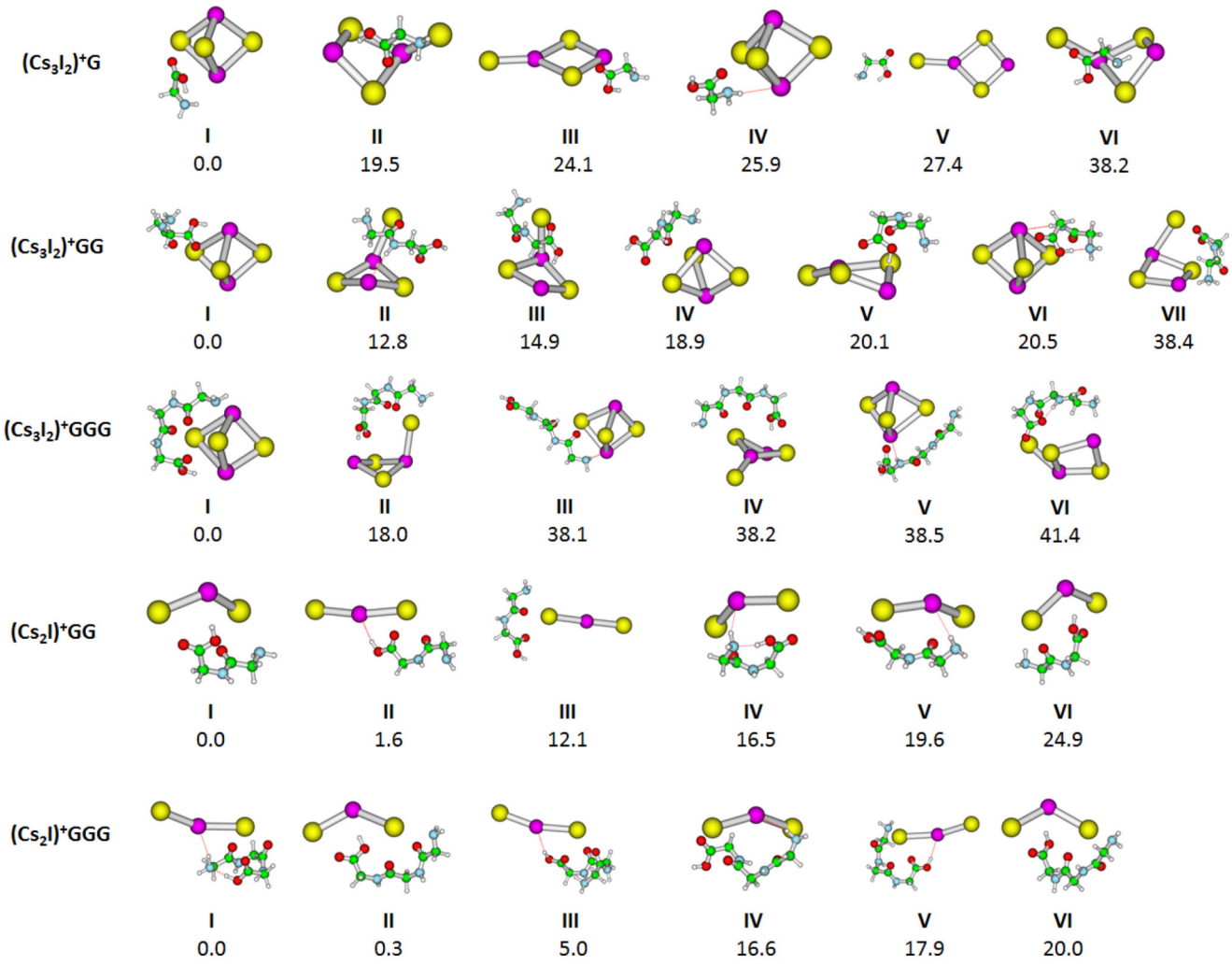

Figure 1.

Calculated structure of studied ions. Optimized at the MP2/def2SVP+ECP(Cs,I) level of theory, relative energy including zero-point corrections is given in kJ/mol.

Europe PMC Funders Author Manuscripts

Europe PMC Funders Author Manuscripts

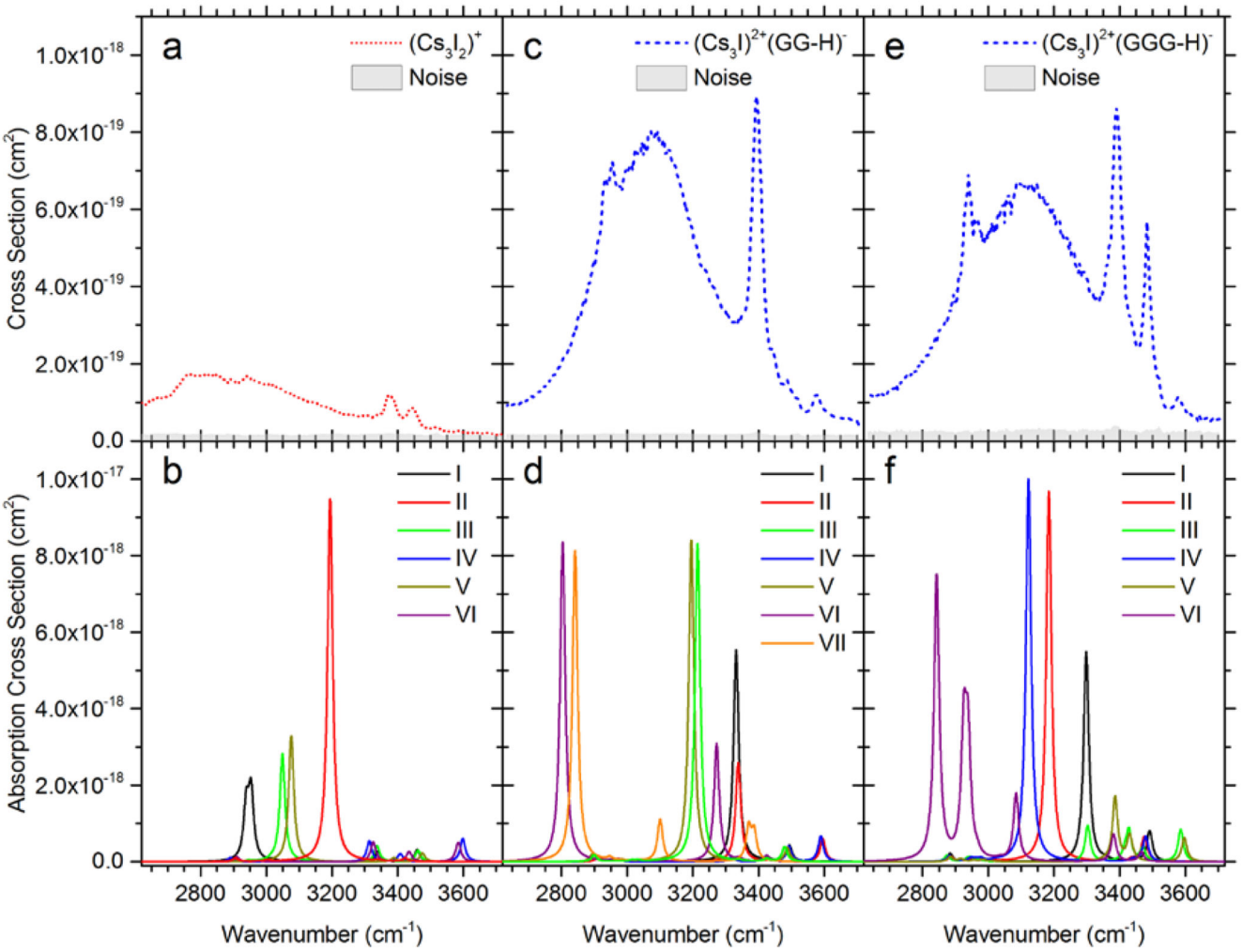

Figure 2.

a,c,e) IRMPD spectra of $(Cs_3I_2)^+G$, $(Cs_3I_2)^+GG$ and $(Cs_3I_2)^+GGG$. Absolute cross sections correspond to the absorption of two photons. b,d,f) Respective IR spectra calculated at the MP2/def2SVP+ECP(Cs,I) level, see Figure 1 for the corresponding isomer structures. Wavenumbers were scaled by a factor of 0.942.

Europe PMC Funders Author Manuscripts

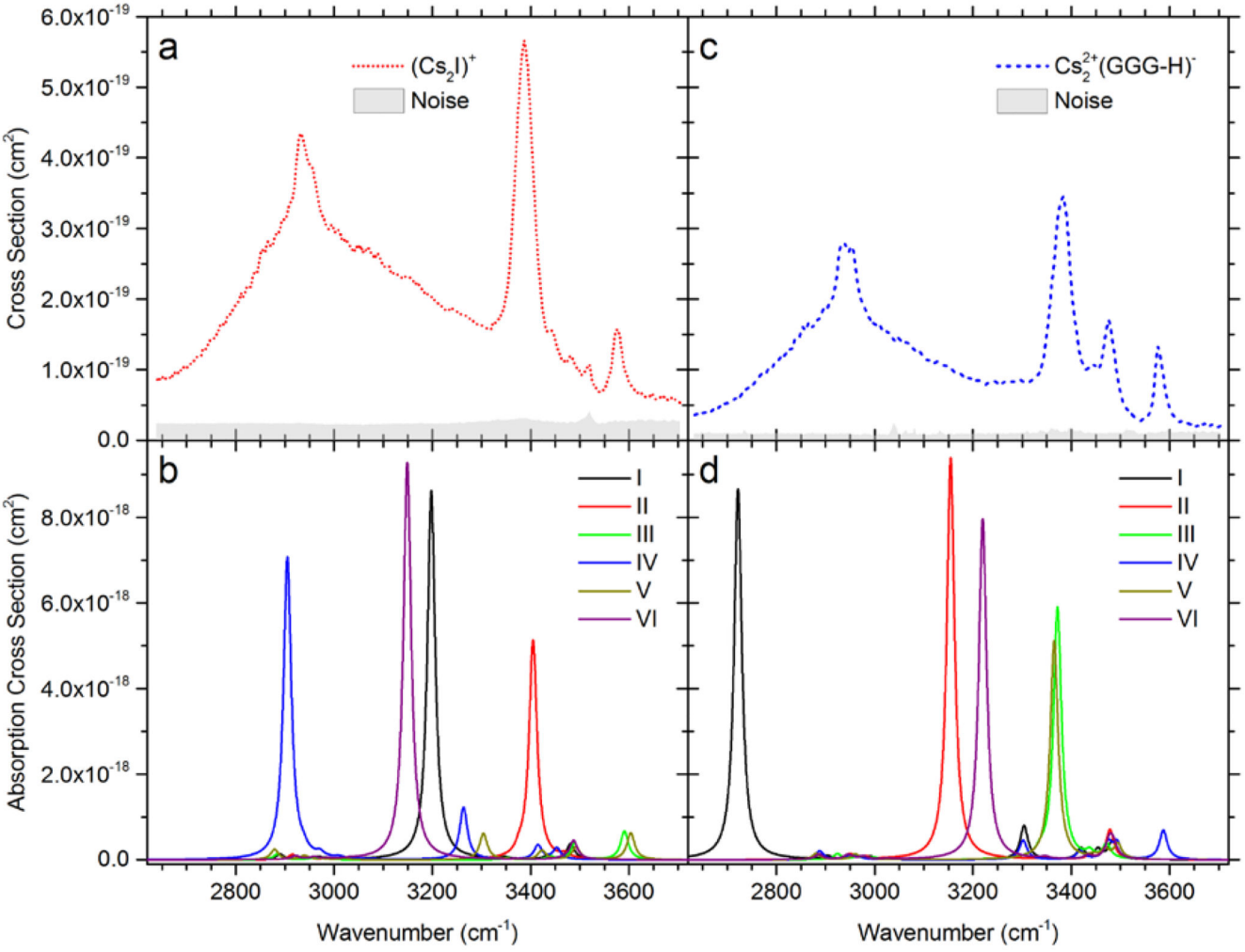

Figure 3.

a,c) IRMPD spectrum of $(Cs_2I)^+GG$ and $(Cs_2I)^+GGG$. Absolute cross sections correspond to the absorption of two photons. b,d) Respective IR spectra calculated at the MP2/def2SVP +ECP(Cs,I) level, see Figure 1 for the corresponding isomer structures. Wavenumbers were scaled by a factor of 0.942.

Europe PMC Funders Author Manuscripts

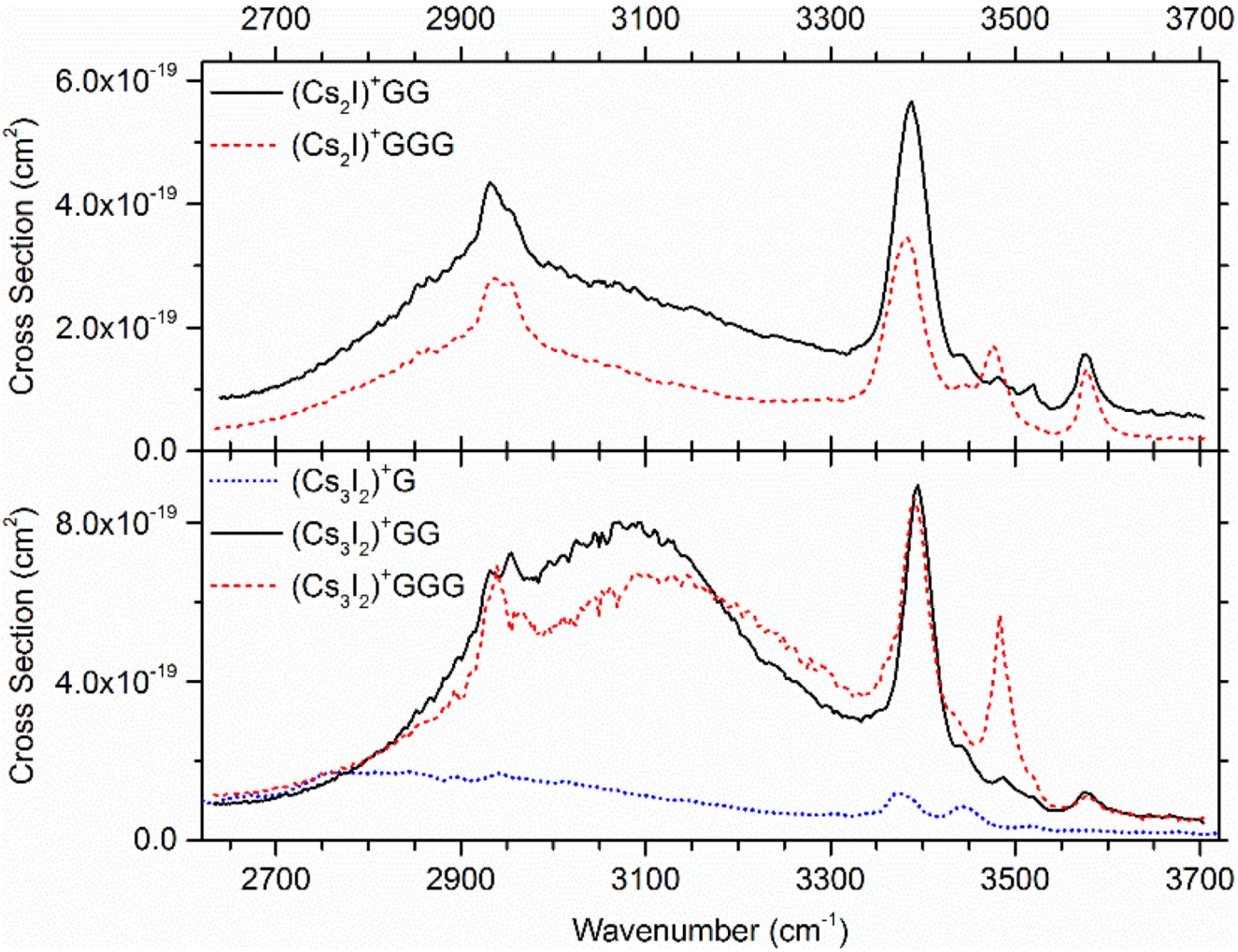

Figure 4.

Comparison of the measured IRMPD spectra. The total IRMPD yields of $(Cs_2I)^+$ complexes are shown in the top row, for $(Cs_3I_2)^+$ complexes in the bottom row. Spectra were evaluated assuming that two photons are needed for dissociation within the IRMPD process. Wavenumbers were scaled by a factor of 0.942.

Europe PMC Funders Author Manuscripts

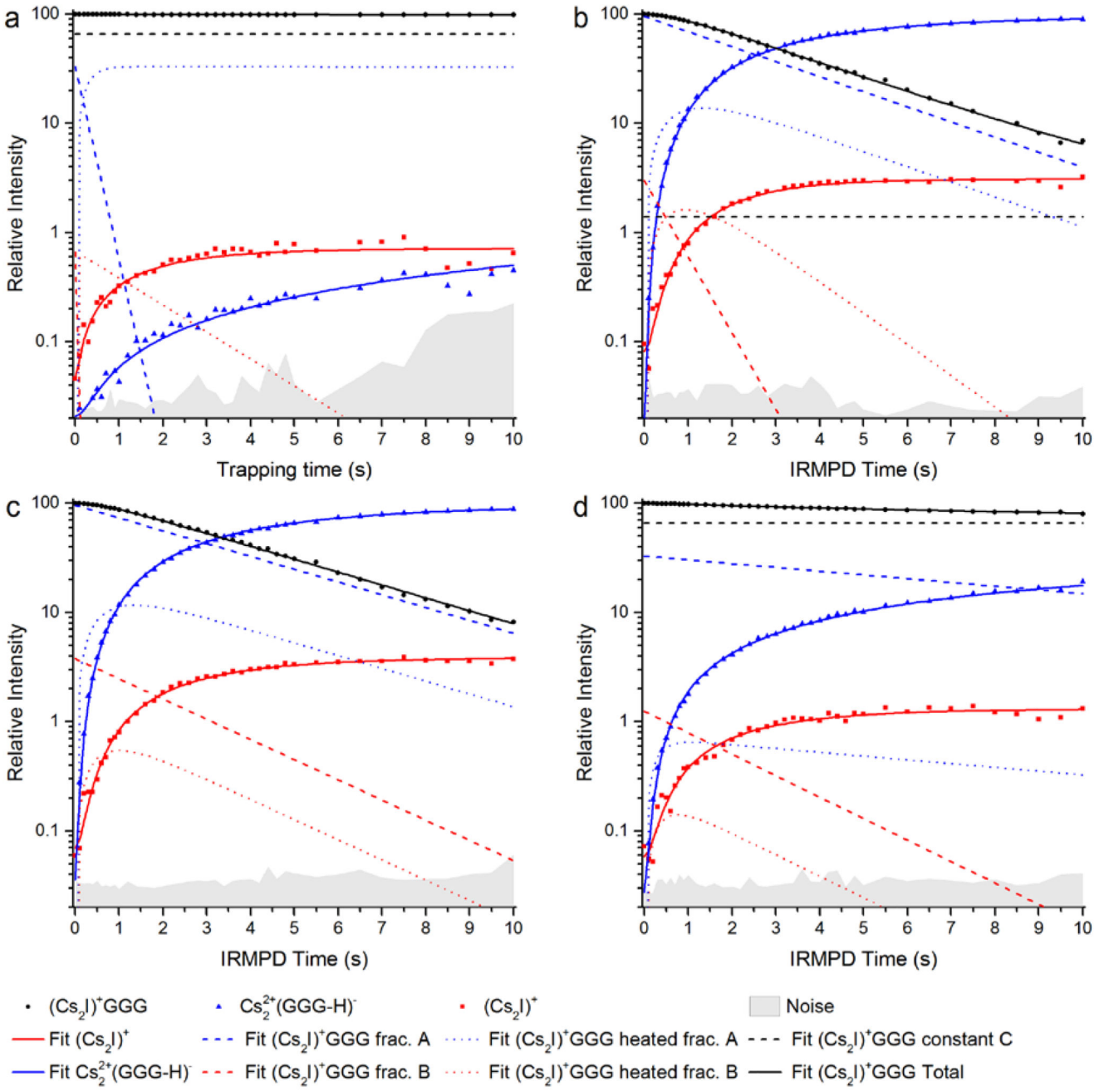

Figure 5.

Dissociation kinetics of $(Cs_2I)^+GGG$ a) without laser irradiation, i.e. fragment formation exclusively due to BIRD; and with the irradiation at b) 2941 cm^{-1}, c) 3390 cm^{-1} and d) 3571 cm^{-1}.

Europe PMC Funders Author Manuscripts

Table 1

Reaction energies (in kJ/mol, including zero-point corrections) of the two evaporation channels observed in the experiment. Calculated at the MP2/def2SVP+ECP(Cs,I) and M06/def2TZVP (in parenthesis) levels of theory.

ion	HI evaporation (4)	glycine (G/GG/GGG) evaporation (5)
$(Cs_3I_2)^+G$	110 (92)	100 (108)
$(Cs_3I_2)^+GG$	84 (48)	126 (111)
$(Cs_3I_2)^+GGG$	98 (83)	151 (167)
$(Cs_2I)^+GG$	114 (104)	111 (124)
$(Cs_2I)^+GGG$	103 (86)	122 (146)